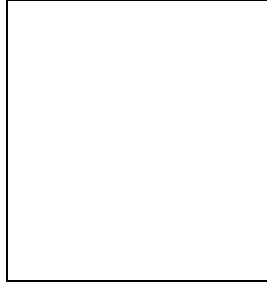


**MEASUREMENT OF FORWARD-BACKWARD ASYMMETRY IN
 $B \rightarrow K^* \ell^+ \ell^-$ AND EVIDENCE OF $B^- \rightarrow \tau^- \bar{\nu}_\tau$**

K. IKADO

*Department of Physics, Nagoya University,
 Nagoya, 464-8602, Japan*



We report the first measurement of the forward-backward asymmetry and the ratios of Wilson coefficients in $B \rightarrow K^* \ell^+ \ell^-$, using 386×10^6 $B\bar{B}$ pairs that were collected on the $\Upsilon(4S)$ resonance with the Belle detector at the KEKB asymmetric-energy e^+e^- collider. We also present the first evidence of the decay $B^- \rightarrow \tau^- \bar{\nu}_\tau$, using 414 fb^{-1} of data.

1 Introduction

Flavor-changing neutral current $b \rightarrow s$ processes proceed via loop diagrams in the Standard Model (SM). The $b \rightarrow s$ processes are sensitive to new physics effect. If new heavy particles can contribute to the decays, their amplitudes will interfere with the SM amplitudes and thereby modify the decay rate as well as decay distributions. Such contributions may change the Wilson coefficients¹ that parametrize the strength of the short distance interactions. The $b \rightarrow s \ell^+ \ell^-$ amplitude is described by the effective Wilson coefficients \tilde{C}_7^{eff} , \tilde{C}_9^{eff} and $\tilde{C}_{10}^{\text{eff}}$. Measurement of the forward-backward asymmetry and differential decay rate as functions of q^2 and θ for $B \rightarrow K^* \ell^+ \ell^-$ constrains the relative signs and magnitudes of these coefficients^{2,3}. Here, q^2 is the squared invariant mass of the dilepton system, and θ is the angle between the momenta of the negative (positive) lepton and the B (\bar{B}) meson in the dilepton rest frame.

The purely leptonic decay $B^- \rightarrow \tau^- \bar{\nu}_\tau$ proceeds via annihilation of b and \bar{u} quarks to a W^- boson in the SM. It provides a direct determination of the product of the B meson decay constant f_B and the magnitude of the Cabibbo-Kobayashi-Maskawa (CKM) matrix element $|V_{ub}|$. The branching fraction is given by

$$\mathcal{B}(B^- \rightarrow \tau^- \bar{\nu}_\tau) = \frac{G_F^2 m_B m_\tau^2}{8\pi} \left(1 - \frac{m_\tau^2}{m_B^2}\right)^2 f_B^2 |V_{ub}|^2 \tau_B, \quad (1)$$

where G_F is the Fermi coupling constant, m_B and m_τ are the B and τ masses, respectively, and τ_B is the B^- lifetime⁴. Purely leptonic B decays have not been observed in past experiments. The most stringent upper limit on $B^- \rightarrow \tau^- \bar{\nu}_\tau$ comes from the BaBar experiment: $\mathcal{B}(B^- \rightarrow \tau^- \bar{\nu}_\tau) < 2.6 \times 10^{-4}$ (90% C.L.)⁵.

The Belle detector is a large-solid-angle magnetic spectrometer consisting of a silicon vertex detector, a 50-layer central drift chamber (CDC), a system of aerogel threshold Čerenkov counters (ACC), time-of-flight scintillation counters (TOF), and an electromagnetic calorimeter comprised of CsI(Tl) crystals (ECL) located inside a superconducting solenoid coil that provides a 1.5 T magnetic field. An iron flux-return located outside of the coil is instrumented to identify K_L^0 and muons. The detector is described in detail elsewhere⁶.

2 Measurement of Forward-Backward Asymmetry in $B \rightarrow K^* \ell^+ \ell^-$

We use a 357 fb^{-1} data sample containing 386×10^6 $B\bar{B}$ pairs taken at the $\Upsilon(4S)$ resonance. We also study the $B^+ \rightarrow K^+ \ell^+ \ell^-$ mode, which is expected to have very small forward-backward asymmetry even in the existence of new physics⁷. The following final states are used to reconstruct B candidates: $K^{*0} \ell^+ \ell^-$, $K^{*+} \ell^+ \ell^-$, and $K^+ \ell^+ \ell^-$, with subdecays $K^{*0} \rightarrow K^+ \pi^-$, $K^{*+} \rightarrow K_S^0 \pi^+$ and $K^+ \pi^0$, $K_S^0 \rightarrow \pi^+ \pi^-$, and $\pi^0 \rightarrow \gamma\gamma$. Hereafter, $K^{*0} \ell^+ \ell^-$ and $K^{*+} \ell^+ \ell^-$ are combined and called $K^* \ell^+ \ell^-$. We use two variables defined in the center-of-mass (CM) frame to select B candidates: the beam-energy constrained mass $M_{bc} \equiv \sqrt{E_{\text{beam}}^2 - p_B^2}$ and the energy difference $\Delta E \equiv E_B - E_{\text{beam}}$, where p_B and E_B are the measured CM momentum and energy of the B candidate, and E_{beam} is the CM beam energy. The dominant background consists of $B\bar{B}$ events where both B mesons decay semileptonically. We suppress this using missing energy and $\cos\theta_B^*$, where θ_B^* is the angle between the flight direction of the B meson and the beam axis in the CM frame. Backgrounds from $B \rightarrow J/\psi X_s, \psi(2S) X_s$ decays are rejected using the dilepton invariant mass. The signal box is defined as $|M_{bc} - m_B| < 8 \text{ MeV}/c^2$ for both lepton modes and $-55 (-35) \text{ MeV} < \Delta E < 35 \text{ MeV}$ for the electron (muon) mode.

We perform an unbinned maximum-likelihood fit to the M_{bc} distribution to determine the signal yield. The fit function includes signal, cross-feeds and other background components. In the fit, all background fractions except the dilepton background are fixed while the signal fraction is allowed to float. We obtain 113.6 ± 13.0 and 96.0 ± 12.0 signal events for $K^* \ell^+ \ell^-$ and $K^+ \ell^+ \ell^-$, respectively. Figure 1 shows the fit result.

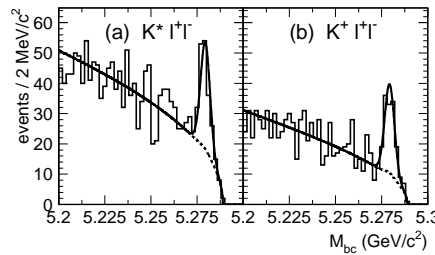


Figure 1: M_{bc} distributions for (a) $B \rightarrow K^* \ell^+ \ell^-$ and (b) $B \rightarrow K^+ \ell^+ \ell^-$ samples. The solid and dashed curves are the fit results for the total and background contributions.

We use $B \rightarrow K^* \ell^+ \ell^-$ candidates in the signal box to measure the normalized double differential decay width. For the evaluation of the Wilson coefficients, the NNLO Wilson coefficients \tilde{C}_i of Ref.⁸ are used. Since the full NNLO calculation only exists for $q^2/m_b^2 < 0.25$ region, we adopt the so-called partial NNLO calculation⁹ for $q^2/m_b^2 > 0.25$. The higher order terms in the \tilde{C}_i are fixed to the SM values while the leading terms A_i , with the exception of A_7 , are allowed to float. Since the branching fraction measurement of $B \rightarrow X_s \gamma$ is consistent with the

prediction within the SM, A_7 is fixed at the SM value, -0.330 , or the sign-flipped value, $+0.330$. We choose A_9/A_7 and A_{10}/A_7 as fit parameters. The SM values for A_9 and A_{10} are 4.069 and -4.213 , respectively⁹. To extract these ratios, we perform an unbinned maximum likelihood fit to the events in the signal box with a probability density function (PDF) that includes the normalized double differential decay width.

We measure the integrated asymmetry \tilde{A}_{FB} , which is defined as

$$\tilde{A}_{\text{FB}} = \frac{\int \int_{-1}^1 \text{sgn}(\cos \theta) g(q^2, \theta) d \cos \theta dq^2}{\int \int_{-1}^1 g(q^2, \theta) d \cos \theta dq^2}. \quad (2)$$

We determine the yield in each q^2 and forward-backward regions from a fit to the M_{bc} distribution. Then we correct the efficiency and obtain

$$\begin{aligned} \tilde{A}_{\text{FB}}(B \rightarrow K^* \ell^+ \ell^-) &= 0.50 \pm 0.15 \pm 0.02, \\ \tilde{A}_{\text{FB}}(B^+ \rightarrow K^+ \ell^+ \ell^-) &= 0.10 \pm 0.14 \pm 0.01, \end{aligned} \quad (3)$$

where the first error is statistical and the second is systematic. A large integrated asymmetry is observed for $K^* \ell^+ \ell^-$ with a significance of 3.4σ . The result for $K^+ \ell^+ \ell^-$ is consistent with zero as expected. The fit results of ratios of Wilson coefficients are summarized in Table 1. Figure 2 shows the fit results projected onto the background-subtracted forward-backward asymmetry distribution in bins of q^2 .

Table 1: A_9/A_7 and A_{10}/A_7 fit results for negative and positive A_7 values. The first error is statistical and the second is systematic.

	Negative A_7	Positive A_7
A_9/A_7	$-15.3^{+3.4}_{-4.8} \pm 1.1$	$-16.3^{+3.7}_{-5.7} \pm 1.4$
A_{10}/A_7	$10.3^{+5.2}_{-3.5} \pm 1.8$	$11.1^{+6.0}_{-3.9} \pm 2.4$

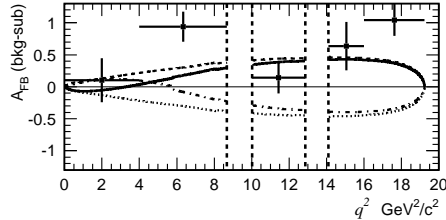


Figure 2: Fit result for the negative A_7 solution (solid) projected onto the background-subtracted forward-backward asymmetry, and forward-backward asymmetry curves for several input parameters, including the effects of efficiency; A_7 positive case ($A_7 = 0.330$, $A_9 = 4.069$, $A_{10} = -4.213$) (dashed), A_{10} positive case ($A_7 = -0.280$, $A_9 = 2.419$, $A_{10} = 1.317$) (dot-dashed) and both A_7 and A_{10} positive case ($A_7 = 0.280$, $A_9 = 2.219$, $A_{10} = 3.817$) (dotted). The new physics scenarios shown by the dot-dashed and dotted curves are excluded.

The fit results are consistent with the SM values $A_9/A_7 = -12.3$ and $A_{10}/A_7 = 12.8$. In Fig. 3, we show confidence level (CL) contours in the $(A_9/A_7, A_{10}/A_7)$ plane based on the fit likelihood smeared by the systematic error, which is assumed to have a Gaussian distribution. We also calculate an interval in $A_9 A_{10}/A_7^2$ at the 95% CL for the allowed A_7 region,

$$-14.0 \times 10^2 < A_9 A_{10}/A_7^2 < -26.4. \quad (4)$$

From this, the sign of $A_9 A_{10}$ must be negative, and the solutions in quadrants I and III of Fig. 3 are excluded at 98.2% confidence level. Since solutions in both quadrants II and IV are allowed,

we cannot determine the sign of A_7A_{10} . Figure 2 shows the comparison between the fit results for the negative A_7 value projected onto the forward-backward asymmetry, and the forward-backward asymmetry distributions for several input parameters. We exclude the new physics scenarios shown by the dotted and dot-dashed curves, which have a positive A_9A_{10} value.

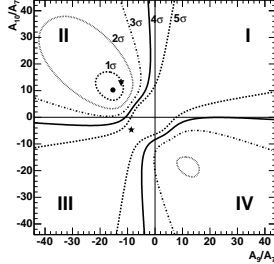


Figure 3: Confidence level contours for negative A_7 . Curves show 1σ to 5σ contours. The symbols show the fit (circle), SM (triangle), and A_{10} -positive (star) cases.

3 Evidence of the Purely Leptonic Decay $B^- \rightarrow \tau^- \bar{\nu}_\tau$

We use a 414 fb^{-1} data sample containing 447×10^6 B meson pairs collected with the Belle detector. We use a detailed MC simulation, which fully describes the detector geometry and response based on GEANT¹⁰, to determine the signal selection efficiency and study the background. The $B^- \rightarrow \tau^- \bar{\nu}_\tau$ signal decay is generated by the EvtGen package¹¹. To model the background from $e^+e^- \rightarrow B\bar{B}$ and continuum $q\bar{q}$ ($q = u, d, s, c$) production processes, large $B\bar{B}$ and $q\bar{q}$ MC samples corresponding to about twice the data sample are used.

We fully reconstruct one of the B mesons in the event, referred to hereafter as the tag side (B_{tag}), and compare properties of the remaining particle(s), referred to as the signal side (B_{sig}), to those expected for signal and background. In the events where a B_{tag} is reconstructed, we search for decays of B_{sig} into a τ and a neutrino. Candidate events are required to have one or three charged track(s) on the signal side with the total charge being opposite to that of B_{tag} . The τ lepton is identified in the five decay modes, $\mu^- \bar{\nu}_\mu \nu_\tau$, $e^- \bar{\nu}_e \nu_\tau$, $\pi^- \nu_\tau$, $\pi^- \pi^0 \nu_\tau$ and $\pi^- \pi^+ \pi^- \nu_\tau$, which taken together correspond to 81% of all τ decays⁴. The muon, electron and charged pion candidates are selected based on information from particle identification devices. For all modes except $\tau^- \rightarrow \pi^- \pi^0 \nu_\tau$, we reject events with π^0 mesons on the signal side.

The most powerful variable for separating signal and background is the remaining energy in the ECL, denoted as E_{ECL} , which is sum of the energy of photons that are not associated with either the B_{tag} or the π^0 candidate from the $\tau^- \rightarrow \pi^- \pi^0 \nu_\tau$ decay. For signal events, E_{ECL} must be either zero or a small value arising from beam background hits, therefore, signal events peak at low E_{ECL} . On the other hand background events are distributed toward higher E_{ECL} due to the contribution from additional neutral clusters. The E_{ECL} signal region is optimized for each τ decay mode based on the MC simulation, and is defined by $E_{\text{ECL}} < 0.2$ GeV for the $\mu^- \bar{\nu}_\mu \nu_\tau$, $e^- \bar{\nu}_e \nu_\tau$ and $\pi^- \nu_\tau$ modes, and $E_{\text{ECL}} < 0.3$ GeV for the $\pi^- \pi^0 \nu_\tau$ and $\pi^- \pi^+ \pi^- \nu_\tau$ modes. The E_{ECL} sideband region is defined by $0.4 \text{ GeV} < E_{\text{ECL}} < 1.2 \text{ GeV}$ for the $\mu^- \bar{\nu}_\mu \nu_\tau$, $e^- \bar{\nu}_e \nu_\tau$ and $\pi^- \nu_\tau$ modes, and by $0.45 \text{ GeV} < E_{\text{ECL}} < 1.2 \text{ GeV}$ for the $\pi^- \pi^0 \nu_\tau$ and $\pi^- \pi^+ \pi^- \nu_\tau$ modes. Table 2 shows the number of events found in the sideband region for data ($N_{\text{side}}^{\text{obs}}$) and for the background MC simulation ($N_{\text{side}}^{\text{MC}}$). Table 2 also shows the number of the background MC events in the signal region ($N_{\text{sig}}^{\text{MC}}$). In order to validate the E_{ECL} simulation, we use a control sample of events (double tagged events), where the B_{tag} is fully reconstructed as described above and B_{sig} is reconstructed in the decay chain, $B^- \rightarrow D^{*0} \ell^- \bar{\nu}$ ($D^{*0} \rightarrow D^0 \pi^0$), followed by $D^0 \rightarrow K^- \pi^+$ or

$K^- \pi^- \pi^+ \pi^+$ where ℓ is a muon or electron. Figure 4 shows the E_{ECL} distribution in the control sample for data and the MC simulation scaled to equivalent integrated luminosity in data.

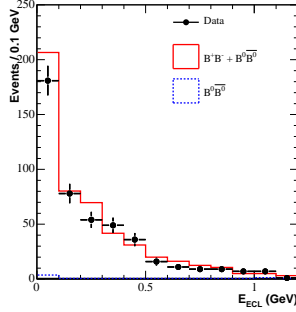


Figure 4: E_{ECL} distribution for the both B tagged events, where one B is fully reconstructed and the other B is reconstructed as $B^- \rightarrow D^{*0} \ell^- \bar{\nu}$. The dots with errors indicate the data. The solid histogram represents the background from $B\bar{B}$ MC ($B^+ B^- + B^0 \bar{B}^0$), and the dashed histogram shows the contribution from $B^0 \bar{B}^0$ events.

After finalizing the signal selection criteria, the signal region is examined. Figure 5 shows the obtained E_{ECL} distribution when all τ decay modes are combined. One can see a significant excess of events in the E_{ECL} signal region below $E_{\text{ECL}} < 0.25$ GeV. Table 2 shows the number of events observed in the signal region (N_{obs}) for each τ decay mode.

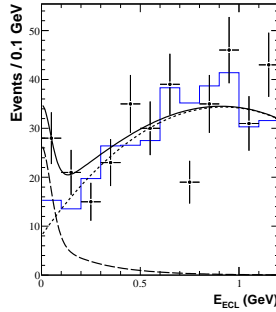


Figure 5: E_{ECL} distributions in the data after all selection requirements have been applied. The data and background MC samples are represented by the points with error bars and the solid histogram, respectively. The solid curve shows the result of the fit with the sum of the signal shape (dashed) and background shape (dotted).

We deduce the final results by fitting the obtained E_{ECL} distributions to the sum of the expected signal and background shapes. Probability density functions (PDFs) for the signal $f_s(E_{\text{ECL}})$ and for the background $f_b(E_{\text{ECL}})$ are constructed for each τ decay mode from the MC simulation. The signal PDF is modeled as the sum of a Gaussian function, centered at $E_{\text{ECL}} = 0$, and an exponential function. The background PDF, as determined from the MC simulation, is parametrized by a second-order polynomial. The results are listed in Table 2. The number of signal events in the signal region deduced from the fit (N_s) is $21.2^{+6.7}_{-5.7}$ when all τ decay modes are combined. Table 2 also gives the number of background events in the signal region deduced from the fit (N_b), which is consistent with the expectation from the background MC simulation ($N_{\text{sig}}^{\text{MC}}$).

The branching fractions are calculated as $\mathcal{B} = N_s / (2 \cdot \varepsilon \cdot N_{B^+ B^-})$ where $N_{B^+ B^-}$ is the number of $\Upsilon(4S) \rightarrow B^+ B^-$ events, assumed to be half of the number of produced B meson pairs. The efficiency is defined as $\varepsilon = \varepsilon^{\text{tag}} \times \varepsilon^{\text{sel}}$, where ε^{tag} is the tag reconstruction efficiency for events with $B^- \rightarrow \tau^- \bar{\nu}_\tau$ decays on the signal side, and ε^{sel} is the event selection efficiency

	$N_{\text{side}}^{\text{obs}}$	$N_{\text{side}}^{\text{MC}}$	$N_{\text{sig}}^{\text{MC}}$	N_{obs}	N_{s}	N_{b}	$\varepsilon^{\text{sel}}(\%)$	$\mathcal{B}(10^{-4})$
$\mu^- \bar{\nu}_\mu \nu_\tau$	96	94.2 ± 8.0	9.4 ± 2.6	13	$5.4^{+3.2}_{-2.2}$	$9.1^{+0.2}_{-0.1}$	8.88 ± 0.05	$1.01^{+0.59}_{-0.41}$
$e^- \bar{\nu}_e \nu_\tau$	93	89.6 ± 8.0	8.6 ± 2.3	12	$3.9^{+3.5}_{-2.5}$	$9.2^{+0.2}_{-0.2}$	8.18 ± 0.05	$0.79^{+0.71}_{-0.49}$
$\pi^- \nu_\tau$	43	41.3 ± 6.2	4.7 ± 1.7	9	$3.4^{+2.6}_{-1.6}$	$4.0^{+0.2}_{-0.1}$	5.79 ± 0.04	$0.96^{+0.74}_{-0.46}$
$\pi^- \pi^0 \nu_\tau$	21	23.3 ± 4.7	5.9 ± 1.9	11	$6.2^{+3.9}_{-2.7}$	$4.2^{+0.3}_{-0.3}$	8.32 ± 0.08	$1.23^{+0.77}_{-0.53}$
$\pi^- \pi^+ \pi^- \nu_\tau$	21	18.5 ± 4.1	4.2 ± 1.6	9	$3.1^{+3.1}_{-2.6}$	$3.7^{+0.3}_{-0.2}$	1.75 ± 0.03	$2.99^{+3.01}_{-2.49}$
Combined	274	266.9 ± 14.3	32.8 ± 4.6	54	$21.2^{+6.7}_{-5.7}$	$30.2^{+0.5}_{-0.4}$	32.92 ± 0.12	$1.06^{+0.34}_{-0.28}$

Table 2: The number of observed events in data in the sideband region ($N_{\text{side}}^{\text{obs}}$), number of background MC events in the sideband region ($N_{\text{side}}^{\text{MC}}$) and the signal region ($N_{\text{sig}}^{\text{MC}}$), number of observed events in data in the signal region (N_{obs}), number of signal (N_{s}) and background (N_{b}) in the signal region determined by the fit, signal selection efficiencies (ε^{sel}), extracted branching fraction (\mathcal{B}) for $B^- \rightarrow \tau^- \bar{\nu}_\tau$. The listed errors are statistical only.

listed in Table 2. When all τ decay modes are combined we obtain a branching fraction of $(1.06^{+0.34}_{-0.28}) \times 10^{-4}$. The branching fraction for each τ decay mode is consistent within error as shown in Table 2.

Systematic errors for the measured branching fraction are associated with the uncertainties in the number of $B^+ B^-$, signal yields and efficiencies. The total fractional uncertainty of the combined measurement is $^{+20.5\%}_{-24.0\%}$, and we measure the branching fraction to be

$$\mathcal{B}(B^- \rightarrow \tau^- \bar{\nu}_\tau) = (1.06^{+0.34}_{-0.28}(\text{stat})^{+0.22}_{-0.25}(\text{sys})) \times 10^{-4}.$$

The significance is 4.0σ when all τ decay modes are combined, where the significance is defined as $\Sigma = \sqrt{-2 \ln(\mathcal{L}_0/\mathcal{L}_{\text{max}})}$, where \mathcal{L}_{max} and \mathcal{L}_0 denote the maximum likelihood value and likelihood value obtained assuming zero signal events, respectively. Here the likelihood function from the fit is convolved with a Gaussian systematic error function in order to include the systematic uncertainty in the signal yield.

Acknowledgments

The author wish to thank the KEKB accelerator group for the excellent operation of the KEKB accelerator.

References

1. See, for example, G. Buchalla *et al.*, Rev. Mod. Phys. **68**, 1125 (1996).
2. E. Lunghi *et al.*, Nucl. Phys. B **568**, 120 (2000).
3. J. L. Hewett and J. D. Wells, Phys. Rev. D **55**, 5549 (1997); A. Ali *et al.*, Z. Phys. C **67**, 417 (1995); N. G. Deshpande *et al.*, Phys. Lett. B **308**, 322 (1993); B. Grinstein *et al.*, Nucl. Phys. B **319**, 271 (1991); W. S. Hou *et al.*, Phys. Rev. Lett. **58**, 1608 (1987).
4. S. Eidelman *et al.* (Particle Data Group), Phys. Lett. B **592**, 1 (2004).
5. B. Aubert (BABAR Collaboration), Phys. Rev. D **73**, 057101 (2006).
6. A. Abashian *et al.* (Belle Collaboration), Nucl. Instrum. Methods Phys. Res., Sect. A **479**, 117 (2002).
7. D. A. Demir *et al.*, Phys. Rev. D **66**, 034015 (2002).
8. H. H. Asatryan *et al.* Phys. Lett. B **507**, 162 (2001).
9. A. Ali *et al.*, Phys. Rev. D **66**, 034002 (2002).
10. R. Brun *et al.*, GEANT3.21, CERN Report DD/EE/84-1 (1984).
11. See the EvtGen package home page, <http://www.slac.stanford.edu/~lange/EvtGen/>.